MATERIALS CHEMISTRY FRONTIERS

RESEARCH ARTICLE

View Article Online
View Journal | View Issue

Cite this: *Mater. Chem. Front.*, 2024, **8**, 1628

Solvent-free synthesis of stable heterostructured-$CsPbBr_3/Cs_2PbBr_5$ assisted by SiO_2 for white light-emitting diodes†

Jisong Yao,* Tianliang Yao, Kaishuai Zhang, Wenxuan Fan, Zhi Yang, Leimeng Xu, Shalong Wang and Jizhong Song *

Continuously improving the stability of lead halide perovskite nanocrystals (NCs) to meet the requirement of industrialization has received tremendous attention. Phase structure modulation or matrix protection has been proven to be a feasible strategy, but these preparations are still hindered by the usage of organic solvents, complex operations, and unsatisfactory batch reproducibility, conflicting with scaled-up production. Here, we have successfully prepared highly stable cesium lead bromide perovskites with superior luminescence properties (photoluminescence quantum yield, PLQY > 80%) by solid-state synthesis using SiO_2 nanospheres as a reaction medium, which present heterostructured-$CsPb_2Br_5/CsPbBr_3$ (H-CPB). Profiting from the dual-phase structure and SiO_2 matrix protection, the as-obtained H-CPB shows high stability with a retained PL of above 90% under continuous UV light irradiation, which is significantly higher than the 42% for the control sample. Importantly, the proposed method features solvent-free, rapid (within 5 mins), and room-temperature synthesis, which could also be used to scale up production evidenced by a batch of 760 g H-CPB powders without compromising their performance. The resulting H-CPB phosphors and commercial red-emitting phosphor coated on blue GaN chips exhibit tunable color temperatures from warm white to cool white, which indicates that the H-CPB perovskites have huge potential for lighting applications.

Received 23rd November 2023,
Accepted 9th January 2024

DOI: 10.1039/d3qm01233f

rsc.li/frontiers-materials

Introduction

Lead halide perovskite nanocrystals (LHP NCs) have emerged as promising materials for various optoelectronic devices, such as light-emitting diodes (LEDs), solar cells, photodetectors, and lasers, due to their excellent photophysical properties (high photoluminescence quantum yields (PLQYs), narrow emission width, tunable emission spectra, *etc.*).[1–6] Moreover, LHP NCs can easily be prepared quickly even at room temperature, reflecting their unique advantages in the synthesis and processing.[7] However, LHP NCs are characterized by very poor stability due to their low formation energy and soft ionic crystal structure.[7–10] Many studies have shown that LHP NCs could quickly lose photoactivity and even decompose when they are exposed to photoirradiation, heat, and humidity, which has limited their further development and practical applications.[11]

Studies have demonstrated that embedding LHP NCs into inorganic matrixes is one of the most effective strategies to improve their stability.[12–15] Particularly, low-dimensional inorganic perovskites, such as two-dimensional (2D) $CsPb_2Br_5$ (referred to as the 2D phase) and zero-dimensional (0D) Cs_4PbBr_6, are effective matrixes for enhancing the stability and luminescent properties of three-dimensional (3D) $CsPbBr_3$ due to their superior stability and high similarity in lattice constants.[16–18] Many research examples have been realized by solution-based chemistry for the synthesis of LHP heterostructures, enabling improved performance of LEDs.[16,19–22] Despite these great progress, a large amount of organic solvents is usually used in the synthetic and purification processes, which is not only harmful but also increases the production cost.[23] In contrast, solid-state reactions can effectively avoid the use of hazardous solvents and tend to form LHP heterostructures, which have recently received increasing attention in the past few years.[24–27] However, solid-state synthesis of LHP heterostructures still suffers from some drawbacks including high temperatures (above 300 °C), complicated preparation processes, and low PL efficiency of perovskite products, which hinder their practical applications.[24,25,28] Although the heterostructured-$Cs_4PbBr_6/CsPbBr_3$ have been recently synthesized at room temperature by mechanochemical synthesis, it

Key Laboratory of Materials Physics of Ministry of Education, School of Physics and Microelectronics, Zhengzhou University, Daxue Road 75, Zhengzhou 450052, China. E-mail: yaojisong@zzu.edu.cn, songjizhong@zzu.edu.cn

† Electronic supplementary information (ESI) available: Experimental details, characterization, and spectroscopic data. See DOI: https://doi.org/10.1039/d3qm01233f

is still necessary to introduce organic solvents into the reaction system when ligand passivation is required to enhance the PL efficiency as well as the synthesis requires rather long reaction times (tens of hours).[24] Therefore, it is imperative to develop a solvent-free, room-temperature, and rapid synthesis method for efficient and stable LHP heterostructures.[29]

Herein, we report a facile all-solid synthesis of stable heterostructured-$CsPb_2Br_5/CsPbBr_3$ (H-CPB) by embedding $CsPbBr_3$ NCs into $CsPb_2Br_5$ matrixes at room temperature. In our synthesis system, SiO_2 was used as a reaction medium to control the nucleation and growth of H-CPB perovskites, which can effectively avoid the use of organic solvents. Moreover, the organic ligands can be easily introduced into the reaction system for passivating the H-CPB perovskites. More importantly, the final products are highly stable in some harsh conditions, *e.g.*, stored in humid air and under UV light

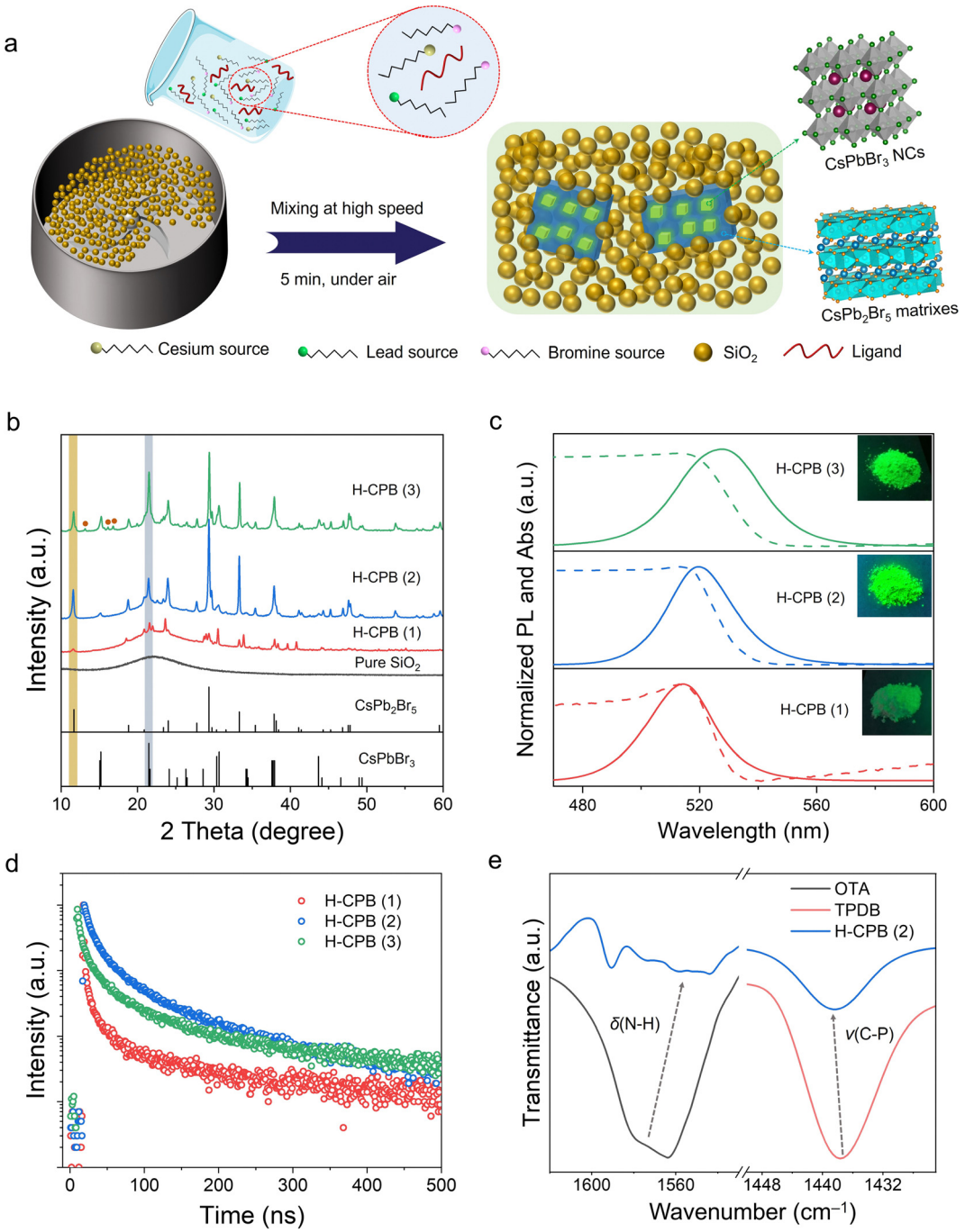

Fig. 1 Preparation and performance of H-CPB composites. (a) Schematic illustration of the fabrication process for H-CPB composites. (b) Powder XRD patterns of pure SiO_2 and H-CPB composites. (c) UV-vis absorption and PL spectra of H-CPB composites. Inset: Photographs of H-CPB composites under the irradiation of UV light (365 nm). (d) PL decay kinetics for H-CPB composites. (e) FTIR spectra of OTA, TPDB, and the H-CPB (2).

irradiation. Finally, we demonstrate that the H-CPB powders can be used as down-converting material for a white LED with tunable color temperature from warm white to cool white. The WLEDs also showed good stability in the air (relative humidity ~ 50%) with minimal change in the emission color during the operation for more than 12 h under the 10-mA driving current.

Results and discussion

H-CPB composites were obtained through a solid-state synthesis, which was quite simple and only required rapid mixing of the raw materials (refers to the materials used to synthesize H-CPB) with SiO_2 powder at room temperature (Fig. 1a). In a typical experiment, guanidine carbonate (Gu_2CO_3) cesium stearate, lead stearate, nickel stearate, octylamine (OTA), and SiO_2 were firstly mixed in a mixer at high speed for 2 min. Then, a certain amount of triphenylphosphine dibromide (TPDB) was added into the above reaction system (molar ratio of Cs : Pb : Br : SiO_2 is 3 : 5 : 15 : 70) and stirred rapidly for 3 min to obtain H-CPB composites. It is worth mentioning that the whole process of the above reaction was carried out in the air without any heating equipment. In order to optimize the performance of the final composites, we prepared three different ratios of LHPs to SiO_2. Hereafter, the products synthesized by inadequate, moderate, and excess LHPs are denoted as H-CPB (1), H-CPB (2), and H-CPB (3), respectively (See ESI† for details). As shown in Fig. 1b, the powder X-ray diffraction (XRD) confirmed the coexistence of monoclinic $CsPbBr_3$ (PDF# 18-0364) and tetragonal $CsPb_2Br_5$ (PDF# 25-0211) in the material system. It can be seen that the diffraction peaks of $CsPbBr_3$ in the CPB/SiO_2 composites were exhibited more significantly as the proportion of SiO_2 decreased. When the proportion of LHPs is in excess (H-CPB (3)), we also observed the diffractions from impurities (marked by brown balls), which may have originated from the raw materials without the reaction. The broad diffraction band ranging from 10° to 30° should be attributed to the existence of amorphous silica, which was consistent with the XRD pattern of pure SiO_2.

The optical properties and surface chemistry of H-CPB composites were further investigated. As shown in Fig. 1c, the H-CPB composites featured green emission peaks at ~520 nm

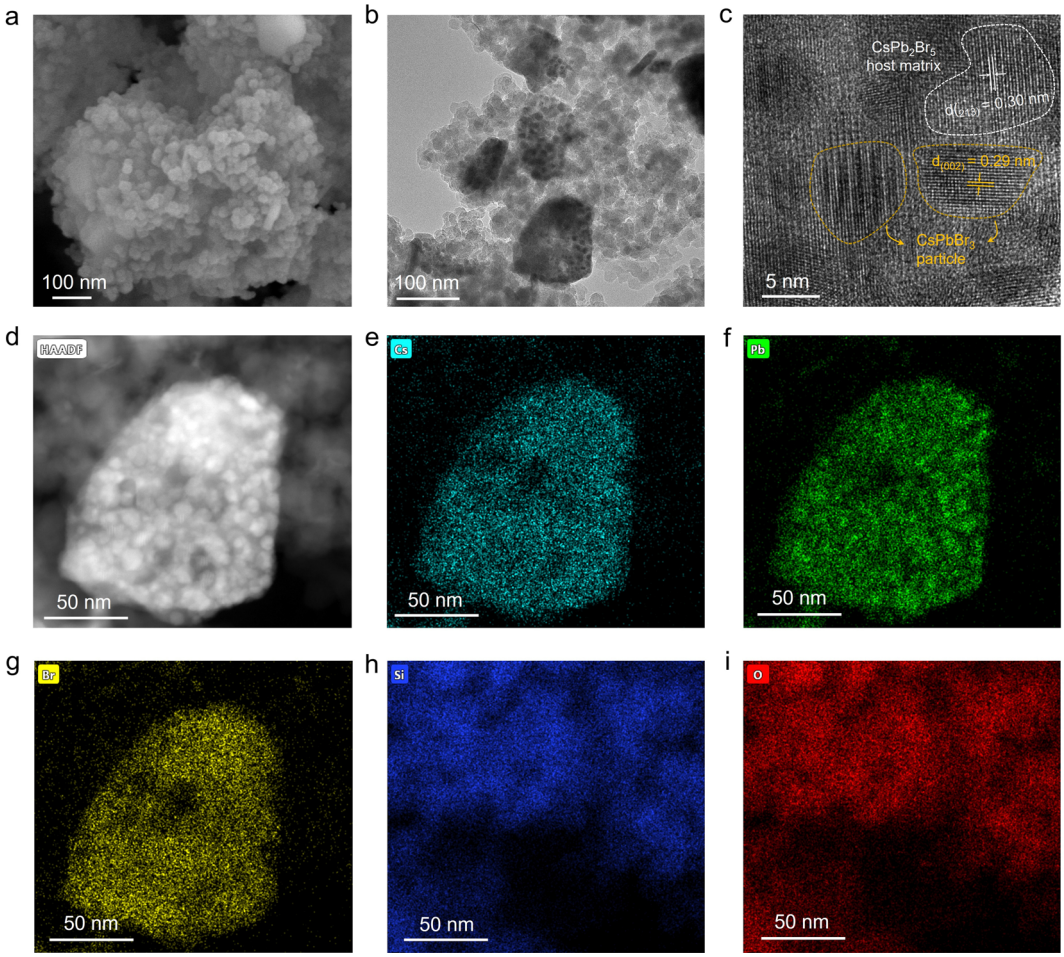

Fig. 2 Microstructural characterization of H-CPB composites. (a) Typical SEM images of H-CPB. (b) SEM images of H-CPB. (c) HRTEM image of $CsPbBr_3$ NCs embedded in $CsPb_2Br_5$. (d)–(i) HAADF-STEM image and the corresponding elemental mapping images showing the elemental distribution of Cs, Pb, Br, Si, and O.

with a narrow full width at half maximum (FWHM) of ~26 nm. A clear red-shift of PL spectra (from 514 to 526 nm) was also seen, which was caused by the larger size of LHP particles according to SEM image results (Fig. 2a and Fig. S1, ESI†). The PLQY values of H-CPB (1), H-CPB (2), and H-CPB (3) were determined to be 15%, 83%, and 54%, respectively, indicating that the ratio of SiO_2 nanospheres plays a key role in regulating the crystallization process of the H-CPB composites. Meanwhile, it can be clearly seen that the H-CPB (2) exhibits brighter luminescence under UV light. The time-resolved PL spectra of the H-CPB powders were also measured (Fig. 1d), and they can be well-fitted by a double-exponential decay function. The corresponding fitted parameters and relevant discussion are shown in Table S1 (ESI†). The obtained average lifetime of the three samples was measured to be 7.9 ns for H-CPB (1), 41.5 ns for H-CPB (2), and 32.0 ns for H-CPB (3), which was consistent with the PLQY results. To further explore the effect of SiO_2 on H-CPB composites, SiO_2 with different specific surface areas was also studied systematically (Fig. S2, ESI†). Hereafter, the products produced by 100 $m^2 g^{-1}$, 170 $m^2 g^{-1}$, and 230 $m^2 g^{-1}$ of SiO_2 nanospheres were denoted by H-CPB (2), H-CPB (4), and H-CPB (5), respectively (details in the Experimental Section). The results from XRD and SEM showed that the SiO_2 with different specific surface areas could act as a reaction medium to promote the formation of H-CPB (Fig. S3 and S4, ESI†). However, when the specific surface area of SiO_2 gradually increased, the optical performance of H-CPB composites gradually decreased, and even the PL spectrum of H-CPB (5) was obviously blue-shifted and broadened (Fig. S5, ESI†). We further measured Fourier-transform infrared spectroscopy (FTIR) on the as-prepared samples, as depicted in Fig. 1e. Comparing with the raw material ligands, FTIR reveals that the amino group scissoring vibration $\delta(NH_2)$ of OTA and the stretching vibration ν(C–P) of TPDB are broadened and shift significantly in H-CPB composites, indicating that the unsaturated Pb dangling bonds due to halide vacancy can be passivated by OTA and TPDB ligands. In addition, the characteristic vibrational band of N–H bending (1630 cm^{-1}) was detected on the surface of pure SiO_2 nanospheres (Fig. S6, ESI†), which also favors the formation of highly luminescent H-CPB composites.[30]

To reveal the morphology and the structure of H-CPB composites, we performed scanning electron microscopy (SEM) and transmission electron microscopy (TEM) analysis. Hereafter, we will focus on analyzing H-CPB (2) composites as a representative to show the advantages of our proposed method. As shown in Fig. S2 (ESI†), the pure SiO_2 nanospheres have a size of about tens of nanometers. In contrast, the H-CPB composites showed complexes of SiO_2 nanospheres and larger crystalline particles (Fig. 2a), indicating that the large particles belong to H-CPB combined with the XRD analysis. Moreover, the H-CPB particles were wrapped by SiO_2 nanospheres and the number of H-CPB particles also increased with the proportion of introducing raw materials (Fig. S1, ESI†). The TEM image also showed that the H-CPB particles were present between the SiO_2 nanospheres (Fig. 2b). Furthermore, we found that the smaller nanoparticles of about ten nanometers were distributed inside the H-CPB particles. Consistent with this result, the high-resolution TEM (HRTEM) image indicated a mixture of tetragonal and monoclinic lattice fringes corresponding to 2D $CsPb_2Br_5$ and 3D $CsPbBr_3$ phases, respectively, indicating the presence of H-CPB (Fig. 2c). High-angle annular dark-field

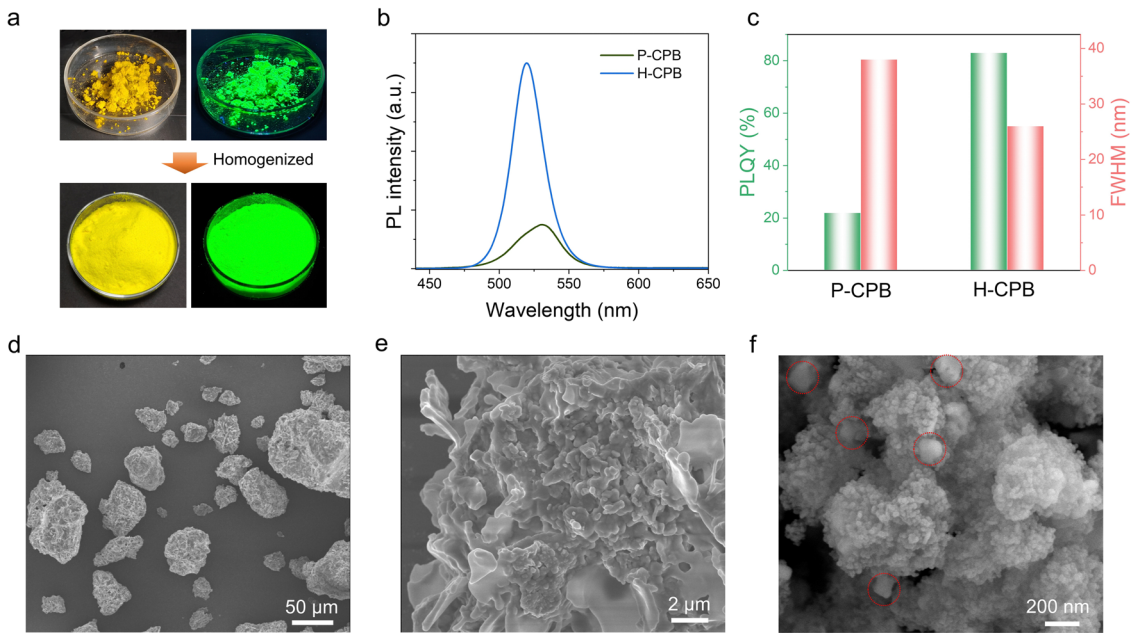

Fig. 3 Improving the homogeneity and PLQYs of CPB composites assisted by SiO_2 nanospheres. (a) Photographs of P-CPB (top) and H-CPB (bottom) under the irradiation of daylight and UV light (right, 365 nm). (b) PL spectra of P-CPB and H-CPB. (c) PLQY value and FWHM of P-CPB and H-CPB. (d) Typical SEM image of P-CPB. (e) High-magnification SEM image of P-CPB. (f) Typical SEM image of H-CPB composites.

scanning transmission electron microscopy (HAADF-STEM) (Fig. 2d) and energy-dispersive X-ray spectroscopy (EDS) (Fig. 2e–i) were used to reveal the elemental distribution. The elements Cs, Pb, and Br elements were homogeneously distributed in the H-CPB part, and Si and O elements were deposited around it. Furthermore, the quantification of the EDS spectrum revealed a Cs : Pb : Br atomic ratio of 1 : 1.92 : 3.77 (this ratio is between the corresponding $CsPbBr_3$ of 1 : 1:3 and $CsPb_2Br_5$ of 1 : 2:5) in the as-synthesized H-CPB (Fig. S7, ESI†), further indicating the formation of $CsPb_2Br_5$/$CsPbBr_3$ heterostructures.

To demonstrate the role of SiO_2 as a reaction medium, we further investigated the direct synthesis of LHPs without SiO_2 (denoted as pure CPB (P-CPB)). As can also be seen from the photographs of P-CPB (Fig. 3a), the dark yellow powders are agglomerated. On a relative basis, the H-CPB powders showed more homogeneity and emitted a brighter green light. Moreover, as shown in Fig. 3b and c, the P-CPB features an asymmetric peak at ~530 nm with a broader FWHM of ~36 nm and lower PLQY of 22% compared to the H-CPB composites (FWHM = 26 nm, PLQY = 83%), which showed that the SiO_2 as a reaction medium can sufficiently homogenize CPB particles and improve their PL efficiency. The crystal structure of the P-CPB was evaluated using XRD analysis (Fig. S8, ESI†). Diffraction peaks proved that the P-CPB contains some impurities (marked by purple crosses) that may have originated from unreacted salts in addition to the coexistence of monoclinic $CsPbBr_3$ and tetragonal $CsPb_2Br_5$, which further demonstrates the role of SiO_2 as a mediator in promoting LHP generation in the solid-state reactions. Furthermore, the low-magnification SEM image showed that the P-CPB is composed of irregular micron-sized particles (Fig. 3d). Moreover, the high-magnification SEM image shows noticeable wrinkles on the surface of the P-CPB, which is different from that of the H-CPB composites (Fig. 3e and f). In addition, the TEM analysis further confirmed that $CsPbBr_3$ NCs were embedded in the $CsPb_2Br_5$ matrix in the pure CPB (Fig. S9, ESI†), which is consistent with the XRD results. As a result, the SiO_2 nanospheres not only play a role in promoting the formation of the $CsPb_2Br_5$/$CsPbBr_3$ heterostructures but also effectively avoids the agglomeration of products, enabling high-quality LHP heterostructures.

In order to meet the needs of commercial applications, LHP NCs are supposed to be stable under practical application situations. Therefore, we studied the stability of H-CPB composites upon storage and light irradiation under ambient conditions. The PL spectra of H-CPB hardly change at all even after storage for 100 days and could maintain 95% of the original PLQY (Fig. 4a). Furthermore, the photostability test of H-CPB, P-CPB, and colloidal $CsPbBr_3$ NCs was implemented under continuous UV light irradiation (365 nm, 106 mW cm^{-2}). As shown in Fig. 4b, the relative PL intensity of P-CPB and colloidal $CsPbBr_3$ NCs was decreased to 42% and 10% of the initial intensity after the light irradiation for 100 h, respectively. On the contrary, the relative PL intensity of H-CPB composites was still maintained above 90%, and no obvious PL decrease was observed under irradiation for 100 h (Fig. S10, ESI†). To assess the environmental stability of H-CPB composites, water

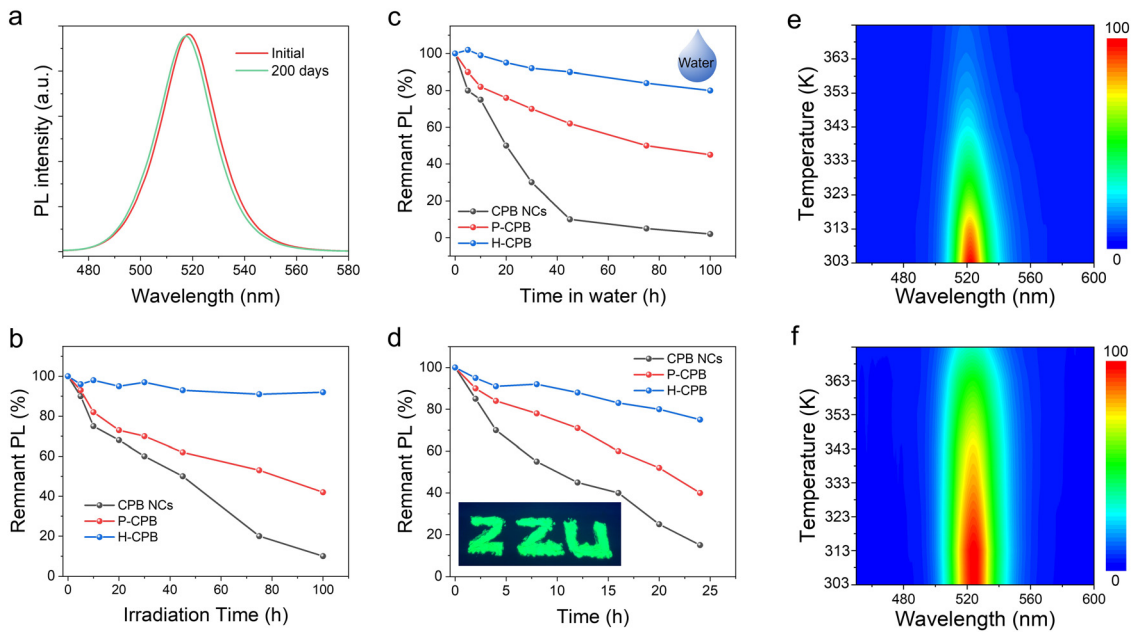

Fig. 4 PL stability tests on $CsPbBr_3$ NCs, P-CPB, and H-CPB composites. (a) PL spectra of H-CPB composites before and after storing in air (25 °C and humidity of 50%) for 100 days. (b) Change in PL intensity of $CsPbBr_3$ NCs, P-CPB, and H-CPB composites under UV light irradiation (λ = 365 nm, 106 mW cm^{-2}). (c) Change in the PL intensity of $CsPbBr_3$ NCs, P-CPB, and H-CPB composites after immersing in water. (d) Change in the PL intensity of $CsPbBr_3$ NCs, P-CPB, and H-CPB composites at a high temperature of 85 °C and a humidity of 50%. The inset is the PL emission photograph for H-CPB composites coated on the surface of a dust-free cloth. (e) Pseudo-color maps of the temperature-dependent PL spectra of $CsPbBr_3$ NCs. (f) Pseudo-color maps of the temperature-dependent PL spectra of the H-CPB composites.

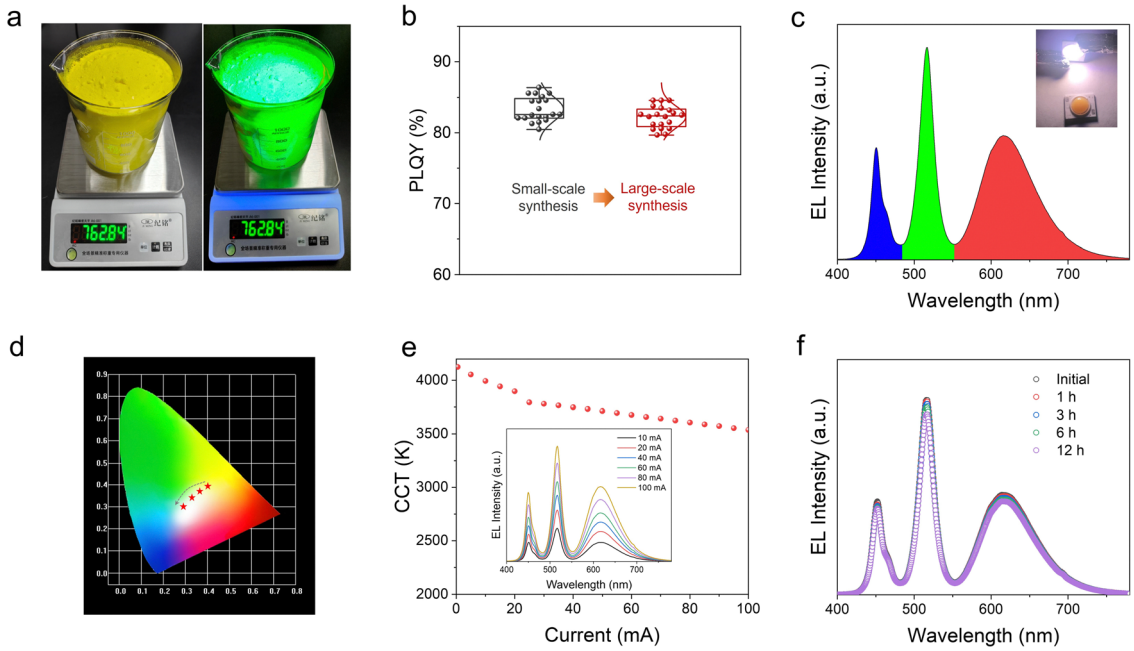

Fig. 5 Large-scale synthesis of H-CPB composites for WLEDs. (a) Photographs of the large-scale synthesized H-CPB powders. (b) Statistical PLQY distribution for small-scale and large-scale synthesis of H-CPB composites. (c) EL spectrum of H-CPB composite-based WLEDs operated at 10 mA (inset: The photograph of the WLED). (d) CIE color diagram of the WLEDs. (e) CCT of the WLEDs under different driving currents. Inset is EL spectra of WLEDs as a function of operating current. (f) EL spectra of WLEDs under continuous current of 10 mA measured at different continuous working times.

tolerance tests were carried out by immersing $CsPbBr_3$ NCs, C-CPB, and H-CPB composites in water under ambient conditions (Fig. 4c). It should be pointed out that the $CsPbBr_3$ NCs, C-CPB, and H-CPB composites are encapsulated in UV-curing resin. It was observed that the relative PL intensity of $CsPbBr_3$ NCs was decreased to 15% and the green-light emission completely disappeared after being immersed in water for 100 hours. In striking contrast, the H-CPB composites could still maintain 80% of the initial PL intensity value. In addition, the thermal stability tests were carried out by monitoring the variation of the PL intensity of the sample before and after annealing at 85 °C for 24 h under ambient conditions. As depicted in Fig. 4d, the H-CPB composites still maintained 75% of the initial PL intensity value after annealing for 24 h. However, the relative PL intensity of $CsPbBr_3$ NCs decreased to 15% and was almost completely quenched after 24 h. Meanwhile, the H-CPB composites exhibited higher stability with increasing temperatures from 30 to 100 °C (Fig. 4e and f). The above results clearly show that the H-CPB composites could significantly improve the stability of LHP NCs due to the synergistic effect of dual-phase structure and SiO_2 matrix protection, which could also promote their practical applications.

The high stability and efficiency of H-CPB composites make them promising candidates for white LEDs (WLEDs). More remarkably, by simply increasing the batch size, this proposed solid-state approach can be scaled up to an industrial scale. To support this conclusion, we have successfully prepared a batch size of 760 g for H-CPB composites (Fig. 5a). Moreover, the H-CPB composites demonstrate good performance reproducibility evidenced by the statistical PLQY distribution even when prepared in large batches, as shown in Fig. 5b. Therefore, WLEDs were prepared by pumping the phosphor blend of a commercial red-emitting $CaAlSiN_3:Eu^{2+}$ (CASN) phosphor and H-CPB composites on a 455 nm blue-LED chip. As seen in Fig. 5c, the electroluminescence (EL) spectrum obviously consists of three emission bands of blue, green, and red, which belong to the blue LED chip, H-CPB composites, and CASN phosphor, respectively. The Commission Internationale de L'Eclairage (CIE) chromaticity coordinate of (0.379, 0.386) and a correlated color temperature (CCT) value of 3994 K were obtained for the resulting WLED, which corresponds to an excellent warm white light emission. Meanwhile, the white light ranging from "warm" to "cold" was achieved by simply varying the ratio of green and red phosphors (Fig. 5d). Fig. 5e illustrates the detailed CCT variation and EL spectra under different driving currents. Small changes of CCT increase from 4125 K at 0.5 mA to 3538 K at 100 mA suggest high stability of the obtained WLED device against current variations. WLEDs also showed good stability in the air (relative humidity ~50%) with minimal change in the emission color during the operation for more than 12 h under the 5-mA driving current, as shown in Fig. 5f. These results indicate that the stability of H-CPB composites has been significantly improved.

Conclusion

In summary, we synthesized H-CPB composites in large batches by a quick solid-state reaction under ambient conditions. We demonstrated that the SiO_2 nanospheres can be used as a

reaction medium to control the growth of LHPs, realizing the preparation of H-CPB composites, which exhibit high chemical and optical stability without encapsulation. Benefitting from these excellent properties and high stability, we have combined green H-CPB composites and commercial red phosphors with blue LED chips to obtain WLEDs with excellent stability and adjustable CCT from warm to cool white light. We believe that the H-CPB composites with improved stability and their retaining of excellent optical properties will energetically facilitate their practical applications.

Data availability

All of the necessary data had been included in the ESI.†

Author contributions

J. Y. and J. S. devised the method and conceived the project. J. Y., T. Y., and K. Z. designed and performed the experiments. W. F. carried out the optical measurements. Z.Y., L. X., and S. W. conducted the analytical characterization. J. Y. and J. S. co-wrote the manuscript. All authors contributed to discussions and finalizing the manuscript.

Conflicts of interest

There are no conflicts to declare.

Acknowledgements

This work is supported by National Natural Science Foundation of China (Grant No. 52272166, 22205214, and 12204427), China Postdoctoral Science Foundation (Grant No. 2022M712910), Natural Science Foundation of Henan Province of China (Grant No. 222300420299 and 232300421214), Zhengzhou University Youth Talent Start-up Grant (Grant No. 32340213).

Notes and references

1 T. H. Han, K. Y. Jang, Y. T. Dong, R. H. Friend, E. H. Sargent and T. W. Lee, A roadmap for the commercialization of perovskite light emitters, *Nat. Rev. Mater.*, 2022, **7**, 757–777.
2 M. V. Kovalenko, L. Protesescu and M. I. Bodnarchuk, Properties and potential optoelectronic applications of lead halide perovskite nanocrystals, *Science*, 2017, **358**, 745–750.
3 X. K. Liu, W. Xu, S. Bai, Y. Jin, J. Wang, R. H. Friend and F. Gao, Metal halide perovskites for light-emitting diodes, *Nat. Mater.*, 2021, **20**, 10–21.
4 L. Protesescu, S. Yakunin, M. I. Bodnarchuk, F. Krieg, R. Caputo, C. H. Hendon, R. X. Yang, A. Walsh and M. V. Kovalenko, Nanocrystals of cesium lead halide perovskites ($CsPbX_3$, X = Cl, Br, and I): Novel optoelectronic materials showing bright emission with wide color gamut, *Nano Lett.*, 2015, **15**, 3692–3696.
5 L. N. Quan, F. P. G. de Arquer, R. P. Sabatini and E. H. Sargent, Perovskites for Light Emission, *Adv. Mater.*, 2018, **30**, 1801996.
6 J. S. Yao, L. Wang, K. H. Wang, Y. C. Yin, J. N. Yang, Q. Zhang and H. B. Yao, Calcium-tributylphosphine oxide passivation enables the efficiency of pure-blue perovskite light-emitting diode up to 3.3%, *Sci. Bull.*, 2020, **65**, 1150–1153.
7 Q. A. Akkerman, G. Raino, M. V. Kovalenko and L. Manna, Genesis, challenges and opportunities for colloidal lead halide perovskite nanocrystals, *Nat. Mater.*, 2018, **17**, 394–405.
8 J. W. Hou, P. Chen, A. Shukla, A. Krajnc, T. S. Wang, X. M. Li, R. Doasa, L. H. G. Tizei, B. Chan, D. N. Johnstone, R. J. Lin, T. U. Schulli, I. Martens, D. Appadoo, M. S. Ari, Z. L. Wang, T. Wei, S. C. Lo, M. Y. Lu, S. C. Li, E. B. Namdas, G. Mali, A. K. Cheetham, S. M. Collins, V. Chen, L. Z. Wang and T. D. Bennett, Liquid-phase sintering of lead halide perovskites and metal-organic framework glasses, *Science*, 2021, **374**, 621–625.
9 K. Sun, D. Z. Tan, X. Y. Fang, X. T. Xia, D. J. Lin, J. Song, Y. H. Lin, Z. J. Liu, M. Gu, Y. Z. Yue and J. R. Qiu, Three-dimensional direct lithography of stable perovskite nanocrystals in glass, *Science*, 2022, **375**, 307–310.
10 J. S. Yao, J. J. Wang, J. N. Yang and H. B. Yao, Modulation of metal halide structural units for light emission, *Acc. Chem. Res.*, 2021, **54**, 441–451.
11 H. Cho, Y. H. Kim, C. Wolf, H. D. Lee and T. W. Lee, Improving the stability of metal halide perovskite materials and light-emitting diodes, *Adv. Mater.*, 2018, **30**, 1704587.
12 Y. Duan, C. Ezquerro, E. Serrano, E. Lalinde, J. García-Martínez, J. R. Berenguer and R. D. Costa, Meeting high stability and efficiency in hybrid light-emitting diodes based on SiO_2/ZrO_2 coated $CsPbBr_3$ perovskite nanocrystals, *Adv. Funct. Mater.*, 2020, **30**, 2005401.
13 H. Hu, L. Wu, Y. Tan, Q. Zhong, M. Chen, Y. Qiu, D. Yang, B. Sun, Q. Zhang and Y. Yin, Interfacial synthesis of highly stable $CsPbX_3$/Oxide janus nanoparticles, *J. Am. Chem. Soc.*, 2018, **140**, 406–412.
14 Z. J. Li, E. Hofman, J. Li, A. H. Davis, C. H. Tung, L. Z. Wu and W. Zheng, Photoelectrochemically active and environmentally stable $CsPbBr_3/TiO_2$ core/shell nanocrystals, *Adv. Funct. Mater.*, 2017, **28**, 1704288.
15 A. Loiudice, S. Saris, E. Oveisi, D. T. L. Alexander and R. Buonsanti, $CsPbBr_3$ QD/AlO_x inorganic nanocomposites with exceptional stability in water, light, and heat, *Angew. Chem., Int. Ed.*, 2017, **56**, 10696–10701.
16 S. Bera and N. Pradhan, Perovskite nanocrystal heterostructures: Synthesis, optical properties, and applications, *ACS Energy Lett.*, 2020, **5**, 2858–2872.
17 K. Du, L. He, S. Song, J. Feng, Y. Li, M. Zhang, H. Li, C. Li and H. Zhang, In situ embedding synthesis of highly stable $CsPbBr_3/CsPb_2Br_5$@PbBr(OH) nano/microspheres through water assisted strategy, *Adv. Funct. Mater.*, 2021, **31**, 2103275.

18 L. N. Quan, R. Quintero-Bermudez, O. Voznyy, G. Walters, A. Jain, J. Z. Fan, X. Zheng, Z. Yang and E. H. Sargent, Highly emissive green perovskite nanocrystals in a solid state crystalline matrix, *Adv. Mater.*, 2017, **29**, 1605945.

19 G. K. Grandhi, N. S. M. Viswanath, J. H. In, H. B. Cho and W. B. Im, Robust, brighter red emission from $CsPbI_3$ perovskite nanocrystals via endotaxial protection, *J. Phys. Chem. Lett.*, 2020, **11**, 3699–3704.

20 B. Wang, C. Y. Zhang, S. L. Huang, Z. C. Li, L. Kong, L. Jin, J. H. Wang, K. F. Wu and L. Li, Postsynthesis phase transformation for $CsPbBr_3/Rb_4PbBr_6$ core/shell nanocrystals with exceptional photostability, *ACS Appl. Mater. Interfaces*, 2018, **10**, 23303–23310.

21 J. W. Xu, W. X. Huang, P. Y. Li, D. R. Onken, C. C. Dun, Y. Guo, K. B. Ucer, C. Lu, H. Z. Wang, S. M. Geyer, R. T. Williams and D. L. Carroll, Imbedded nanocrystals of $CsPbBr_3$ in Cs_4PbBr_6: Kinetics, enhanced oscillator strength, and application in light-emitting, *Adv. Mater.*, 2017, **29**, 1703703.

22 X. L. Zhang, B. Xu, J. B. Zhang, Y. Gao, Y. J. Zheng, K. Wang and X. W. Sun, All-inorganic perovskite nanocrystals for high-efficiency light emitting diodes: Dual-phase $CsPbBr_3$-$CsPb_2Br_5$ composites, *Adv. Funct. Mater.*, 2016, **26**, 4595–4600.

23 B. Wang, C. Zhang, W. Zheng, Q. Zhang, Z. Bao, L. Kong and L. Li, Large-scale synthesis of highly luminescent perovskite nanocrystals by template-assisted solid-state reaction at 800 °C, *Chem. Mater.*, 2019, **32**, 308–314.

24 K. Y. Baek, W. Lee, J. Lee, J. Kim, H. Ahn, J. I. Kim, J. Kim, H. Lim, J. Shin, Y. J. Ko, H. D. Lee, R. H. Friend, T. W. Lee, J. Lee, K. Kang and T. Lee, Mechanochemistry-driven engineering of 0D/3D heterostructure for designing highly luminescent Cs-Pb-Br perovskites, *Nat. Commun.*, 2022, **13**, 4263.

25 C. Fan, H. P. Liu, J. W. Zhou, X. L. Dai, H. P. He and Z. Z. Ye, Ultrastable and highly efficient $CsPbBr_3$ composites achieved by dual-matrix encapsulation for display devices, *InfoMat*, 2023, **5**, e12417.

26 A. Karmakar, M. S. Dodd, X. Y. Zhang, M. S. Oakley, M. Klobukowski and V. K. Michaelis, Mechanochemical synthesis of 0D and 3D cesium lead mixed halide perovskites, *Chem. Commun.*, 2019, **55**, 5079–5082.

27 F. Palazon, Y. El Ajjouri, P. Sebastia-Luna, S. Lauciello, L. Manna and H. J. Bolink, Mechanochemical synthesis of inorganic halide perovskites: evolution of phase-purity, morphology, and photoluminescence, *J. Mater. Chem. C*, 2019, **7**, 11406–11410.

28 Z. Y. Zhu, Q. Q. Yang, L. F. Gao, L. Zhang, A. Y. Shi, C. L. Sun, Q. Wang and H. L. Zhang, Solvent-free mechanosynthesis of composition-tunable cesium lead halide perovskite quantum dots, *J. Phys. Chem. Lett.*, 2017, **8**, 1610–1614.

29 K. Zhang, W. Fan, T. Yao, S. Wang, Z. Yang, J. Yao, L. Xu and J. Song, Polymer-surface-mediated mechanochemical reaction for rapid and scalable manufacture of perovskite QD phosphors, *Adv. Mater.*, 2024, 2310521.

30 X. M. Li, Y. Wang, H. D. Sun and H. B. Zeng, Amino-mediated anchoring perovskite quantum dots for stable and low-threshold random lasing, *Adv. Mater.*, 2017, **29**, 1701185.